SCIENCE CHINA
Chemistry

•ARTICLES•

March 2021 Vol.64 No.3: 432–438
https://doi.org/10.1007/s11426-020-9891-4

Optically actuating ultra-stable radicals in a large π-conjugated ligand constructed photochromic complex

Ji-Xiang Hu[1†], Xiao-Fan Jiang[1†], Yu-Juan Ma[1], Xue-Ru Liu[2], Bang-Di Ge[1], A-Ni Wang[1], Qi Wei[1] & Guo-Ming Wang[1*]

[1]*College of Chemistry and Chemical Engineering, Qingdao University, Qingdao 266071, China;*
[2]*Key Laboratory of Synthetic and Natural Functional Molecule Chemistry of the Ministry of Education, College of Chemistry and Materials Science, Northwest University, Xi'an 710069, China*

Received September 17, 2020; accepted October 15, 2020; published online January 18, 2021

Producing ultra-stabilized radicals *via* light irradiation has raised considerable concern but remains a tremendous challenge in functional materials. Herein, optically actuating ultra-stable radicals are discovered in a sterically encumbered and large π-conjugated tri(4-pyridyl)-1,3,5-triazine (TPT) ligands constructed photochromic compound $Cu_3(H\text{-}HEDP)_2TPT_2{\cdot}2H_2O$ (**QDU-12**; HEDP=hydroxyethylidene diphosphonate). The photogeneration of $TPT^{\bullet}$ radicals is the photoactive behavior of electron transfer from HEDP motifs to TPT units. The ultra-long-lived radicals are contributed from strong interchain π-π interactions between the large π-conjugated TPT components, with the radical lifetime maintained for about 18 months under ambient conditions. Moreover, the antiferromagnetic couplings between $TPT^{\bullet}$ radicals and Cu^{2+} ions plummeted the demagnetization to 35% of its original state after light irradiation, showing the largest room temperature photodemagnetization in the current radical-based photochromic materials.

electron transfer, gigantic photodemagnetization, π-conjugated ligands, photochromic, ultra-stable radicals

Citation: Hu JX, Jiang XF, Ma YJ, Liu XR, Ge BD, Wang AN, Wei Q, Wang GM. Optically actuating ultra-stable radicals in a large π-conjugated ligand constructed photochromic complex. *Sci China Chem*, 2021, 64: 432–438, https://doi.org/10.1007/s11426-020-9891-4

1 Introduction

Radicals are an important species in numerous chemical, physical and biological processes [1–4]. In general, radicals acting as fascinating intermediates are typically short-lived and highly reactive due to their labile nature. Stable radicals in chemical systems have booming applications in catalysis, molecular recognition, lithium ions battery, information storage and optoelectronic devices [5–8]. Versatile species of stable radicals have been achieved in organic and organometallic structures, such as oxygen-based radicals, steric-hindrance carbon-centered radicals, nitronyl nitroxide radicals, and spin-delocalized radicals [9–12]. However, it is yet lacking of safety and convenient switch because the generation of stable radicals was largely depended on redox reactions triggered by chemical reagents or electricity [13]. On the other hand, external stimuli operated stable radicals, specially light irradiation, with typically rapid response and convenience of switch on and off, are attracting considerable attention [14,15]. Although it is popular to utilize photon to generate intermediate radicals, it is still in the predicament for directly generating stable radical species by light, which will be in favor of further developing the application of steady-state functional materials.

To generate the radicals and simultaneously stabilize them, structural and electronic features related to radicals should be preferentially considered. Firstly, suitable electron transfer

†These authors contributed equally to this work
*Corresponding author (email: gmwang_pub@163.com)

© Science China Press and Springer-Verlag GmbH Germany, part of Springer Nature 2021

pathways between electron donor/acceptor that could generate and transport radicals should be established upon construction of architectures. Secondly, large π-conjugated ligands act as a crucial part in the kinetic stabilization of free radicals [16]. Spin delocalization, particularly when heteroatoms (N, O, *etc.*) are substituted to the radical centers, also importantly influence the stabilization of generated radicals [17]. Moreover, intermolecular interactions could form condensed coordination networks, further preventing the contact of the generated radicals with oxygen at ambient conditions [18,19].

In this respect, the electron-transfer photochromic complexes undoubtedly can be served as an ideal medium, in which naked-eye detectible color changes are easily observed and relatively stable radicals can be effectively regulated through direct light irradiation. Hitherto, lots of photochromic complexes have been prepared by using the donor-acceptor strategy, exemplified by some inorganic-organic hybrid photochromic frameworks, in which electron-rich inorganic motifs like metallophosphates, polyoxomolybdates and halometallates [20–22] may offer electrons while electron-deficient organic groups [23–25] may be prone to accepting and stabilizing generated radicals. However, it is still a pivotal research challenge for extremely improving the stability of the photogenerated radicals under ambient conditions, which could greatly enhance the catalysis, luminescence and conductivity of the radical-based functional properties.

Herein, ultra-stable radicals *via* light irradiation were discovered in a copper(II)-based compound Cu_3(H-HEDP)$_2$-TPT_2·$2H_2O$ (**QDU-12**; HEDP=hydroxyethylidene diphosphonate, TPT=tri(4-pyridyl)-1,3,5-triazine). The d^9 Cu^{2+} ion and HEDP ligand involving rich O atoms were chosen to construct the HEDP-Cu chain and served as electron donors. The bulky π-conjugated organic TPT ligand could be used as electron acceptors by taking the advantage of its typical electrophilic motif and readily accessible planar backbone, stabilizing the generated radicals *via* spin delocalization and intermolecular stacking interactions. After Xe lamp irradiation, solid state photochromic behavior of **QDU-12** was observed at room temperature. The light-induced coloration was a metal-assisted ligand-to-ligand electron transfer process, and the photogenerated radicals were confirmed by UV-Vis, electron spin resonance (ESR), X-ray photoelectron spectroscopy (XPS) and theoretical calculations. The relaxation process of radicals in **QDU-12A** (the photo-induced colored sample) was studied with UV-Vis and ESR spectra. As a result, the life time of photogenerated radicals was estimated for about 18 months, exhibiting the highest stable charge-separated state compared with the previous reported photochromic complexes. Moreover, the magnetic behaviors were also explored before and after light treatment. The stable generated radicals coupled central Cu^{2+} with obvious antiferromagnetic interactions, pushing demagnetization radio down to 35 % and showing the largest RT demagnetization effect in the photochromic complexes.

2 Results and discussion

Single-crystal X-ray diffraction (SCXRD) analysis revealed the space group $P\bar{1}$ for compound **QDU-12**, with three Cu^{2+} ions, two diphosphonate ligands, two TPT ligands and two lattice water molecules located in the asymmetric unit (Figure 1(a)). All Cu centers were five-coordinated in the distorted spherical square pyramid (Table S4, confirmed by the continuous shape measure analysis, Supporting Information online), with all O atoms from two HEDP units and one N atom from one TPT ligand. The average Cu−O and Cu−N bond lengths were 2.048 and 2.137 Å, respectively, while the elongated bonds along the apical positions (ca. 2.544 Å) were induced by the Jahn-Teller effect, similar with other reported copper(II) complexes [26–28]. Two HEDP ligands connected three Cu^{2+} ions with the same coordination mode of μ^3-η^1:η^1:η^1:η^1:η^1:η^0:η^1, and all the Cu^{2+} ions coordinated with HEDP ligands to form a zigzag chain (Figure S1, Supporting Information online). One bridged TPT ligand bonded with the Cu^{2+} of adjacent chain, while the other terminal coordinated with the chain, forming a parallel double chain structure (Figure S2). Importantly, interchain π-π interactions were formed between terminal TPT ligands among the adjacent double chains, connecting the chains into a supermolecular architecture (Figure 1(b) and S3). Such stacking interactions between π-conjugated organic TPT ligands favor the requirements for electron transfer and provide an efficient strategy for stabilizing the photogenerated radicals.

The combination of both electron donor/acceptor in **QDU-12** may induce photoinduced coloration, thus, illumination experiments by a 100 W Xe lamp were performed at ambient conditions. The compound exhibited significant photo-excited color with high coloration contrasts after irradiated for 1 min (Figure 2(a)), accompanied with the color changed from dark cyan to dark yellow (named as **QDU-12A**). This phenomenon should be due to the generation of free radicals. Interestingly, no visible color bleaching was observed for **QDU-12A** even after thermal annealing at 290 °C, different from the common photochromic complexes with easy discoloration by heating, but still similar with other rarely reported works [19]. Solid-state UV-vis diffuse-reflectance spectra could give more information about the photochromic phenomenon. As a function of irradiation time, the intension of the reflection band at 480 nm progressively weakened and flattened (Figure 2(b)), indicating that the TPT ligand received an electron and formed $TPT^{\bullet}$ radicals after light irradiation. Moreover, this peak moved to higher wave

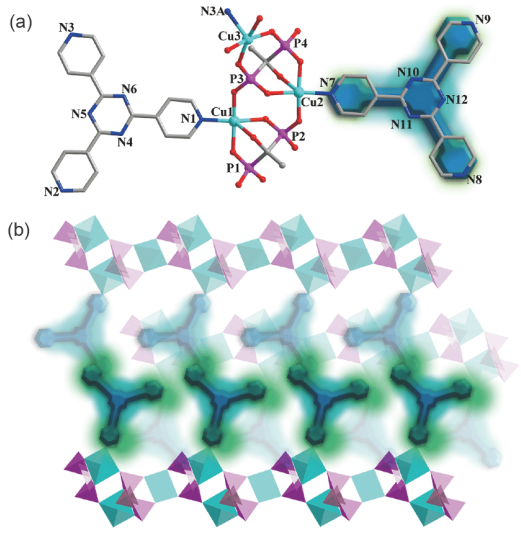

Figure 1 The structure of **QDU-12**. (a) The asymmetric unit; (b) the interchain π-π interactions between the TPT ligands. H atoms and lattice waters are omitted for clarity. Color codes: Cu turquoise; P pink; C gray 40%; O red; N blue (color online).

numbers as the irradiation time increased. The absorption band showed no further clear variation after the sample was irradiated beyond 3 min. To estimate the rate of light-induced coloration, the kinetics of the coloration for **QDU-12** was performed by analyzing the reflectivity of the maximum absorbance wavelength $R(t)$ *versus* irradiation time in the range of 200−800 nm (Figure 2(c)). The curve can be fitted by the function $R^{\lambda max}(t)=a/(bt+1)+R^{\lambda max}(\infty)$ [29,30], with the relative parameters listed in the inset of Figure 2(c). The parameters related to the coloration kinetics a and b are the proportionality constant, and the $R^{\lambda max}(\infty)$ value could reflect the depth of color at the end time of irradiation. In addition, the half-time $t_{1/2}$ (the time required for $R(t)$ to reach the $[R(0)+R(\infty)]/2$ value) could represent the coloration speed, with the value of 12.60 s. The value was quite close to the actual duration to show color transition in the photochromic experiment. The speed of light-induced coloration should be related to the increase of the photogenerated radicals, and the formation of radicals was demonstrated by the following ESR and XPS measurements and molecular orbital calculations. To exclude photoinduced photolysis, isomerization or reduction of Cu^{2+} centers, the crystal structures of **QDU-12** after light irradiation were also analyzed and maintained nearly unchanged with the as-prepared sample, suggesting the formation of stable radicals and confirmed by powder X-ray diffraction (PXRD), infrared radiation (IR) and thermogravimetric (TG) plots (Tables S1−S3 and Figures S4−S6).

In general, the occurrence of the solid-state electron transfer photochromism is mainly originated from H-bonding interactions between the electron donor and acceptor ligands [31]. However, the donor/acceptor units were directly connected by O−Cu−N coordinative bonds for **QDU-12**. These through-bonds could offer the opportunities for the efficient photochromic electron transfer process [32,33]. In fact, **QDU-12** exhibited metal-assisted ligand-to-ligand electron transfer between the two donor/acceptor ligands. The continuous-wave X-band solid-state ESR spectra give more information about the generation of stable radicals. As shown in Figure 2(d), the ESR curves of **QDU-12**

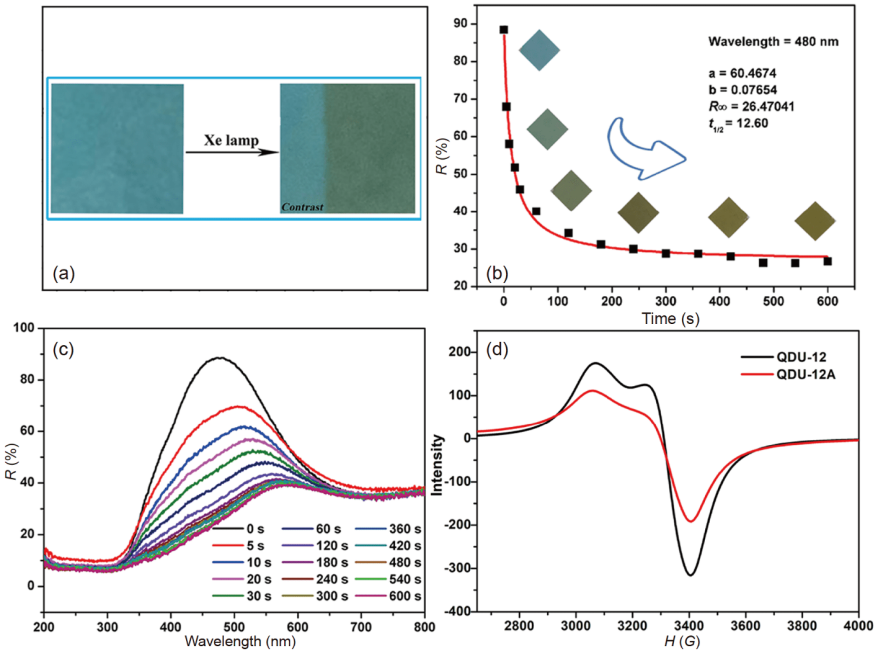

Figure 2 (a) The photochromic phenomenon of powder samples for **QDU-12**; (b) time-dependent UV-Vis diffuse-reflectance spectra of **QDU-12** upon light irradiation; (c) the plot of relative intensity of time-dependent UV-Vis spectra upon light irradiation at 480 nm. The red solid line presented the fitted curve; (d) solid state ESR spectra of **QDU-12** and **QDU-12A** at room temperature (color online).

showed a broad signal with hyperfine splitting at low fields in a frequency of 9.84 GHz, which should be ascribed to Cu^{2+} ions in the distorted square pyramid geometry [34]. However, the ESR signals became much weaker for **QDU-12A**. The anomalies should be attributed to radical formation, and then the photo-induced stable radicals magnetically coupled with Cu^{2+} centers, inducing the weaker ESR signals than the as-prepared **QDU-12** samples [35,36]. The radical generation could also be observed in our previous work [37] and other paramagnetic metal contained photochromic complexes, with the confirmation by the variation of ESR spectra during coloration [19,35,36,38–40].

To give an insight into the electron transfer pathway, the XPS analyses were performed before and after illumination. The Cu and P 2p core-level spectra were almost unchanged, so the Cu centers remained in the II+ valence state. However, the binding energies of the N, O and C spectra exhibited obvious variations during coloration, which were shown in Figure 3. In detail, two N 1s peaks at 399.46 and 403.98 eV ascribed to the TPT ligand in the original state shifted to positions with lower binding energies (399.38 and 403.69 eV), while a higher binding energy position (from 530.71 to 531.39 eV) with a shoulder (532.88 eV) occurred upon going from **QDU-12** to **QDU-12A**. Accompanied with the intensity changes in C 1s binding energies, the XPS results demonstrate the electron transfer process from O atoms of HEDP unit to N atoms of TPT ligand, similar with other reported polypyridine-based photochromic complexes [32,41].

For further corroboration of the photochromic electron transfer processes in **QDU-12**, molecular orbital calculations were performed using the Gaussian 09 program and the basis set B3LYP/6-311G(d) method and adapted from the crystal X-ray data. The calculation results indicated the complete separation of the highest occupied molecular orbital (HOMO) and the lowest unoccupied molecular orbital (LUMO). As shown in Figure 4 and Table S5, the electron distribution of the HOMO was mainly focused on the O atoms from the HEDP units, while the majority of electron distribution for LUMO was located on coordinated pyridine and triazine rings from the TPT moiety. The typical localization of HOMO and LUMO suggests the HOMO-LUMO transition becomes the intramolecular charge transfer transition [42,43]. In other words, the photogenerated $TPT^{\cdot}$ radicals of **QDU-12** should be ascribed to the electron transfer between the oxygen atoms of HEDP group and the N atoms of TPT unit, in good agreement with those of XPS analyses and elucidating the appearence of charge transfer in the photochromic response.

Imporantly, **QDU-12A** exhibited extraordinary stable states for 18 months under ambient conditions. This phenomenon suggested the ultra-long-lived stable radicals after light irradiation, which was crucial for converting solar energy into chemical energy [18]. Moreover, water stability of **QDU-12A** was explored by immersing the compound in water and standing in the dark for 24 h at room temperature. The light generated samples still maintain the same PXRD patterns with the as-prepared crystalline samples (Figure S4), suggesting the high water-stability of the generated radicals in **QDU-12A**. The temperature dependent reflective spectra

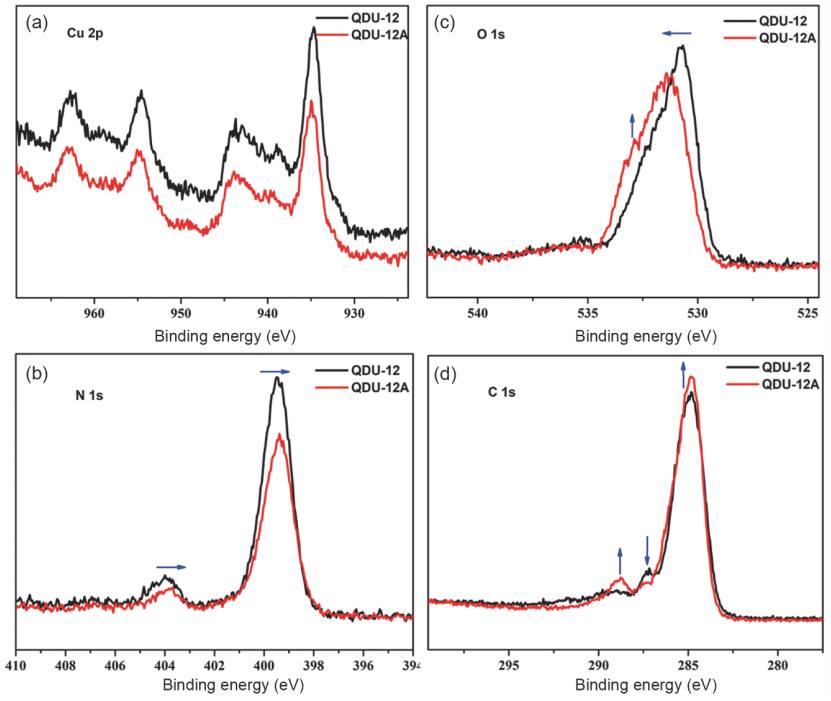

Figure 3 The Cu 2p (a), N 1s (b), O 1s (c) and C 1s (d) of XPS core-level spectra for **QDU-12** and **QDU-12A** (color online).

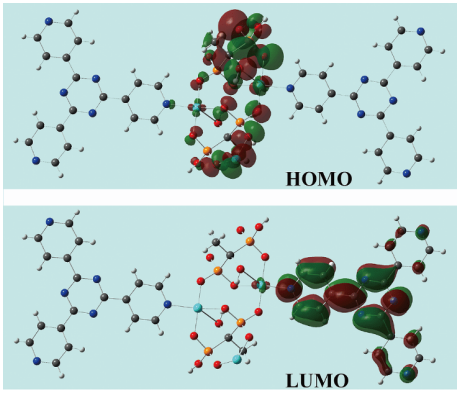

Figure 4 The calculated spatial distributions of LUMO and HOMO of **QDU-12** at the B3LYP/6-311G(d) level (color online).

decay of **QDU-12A** was monitored to check the stability of the photogenerated radicals (Figure 5). The decay of reflective intensity at 560 nm (converted into absorbance) was normalized as photoinduced fraction γ and fitted to a stretched exponential law ($\gamma(t)=\gamma(0)\exp(-t/\tau)^{\beta}$, where τ represents the relaxation time of the system and β represents the factor of time-evolving interactions during the decay process) [44]. A best fitting procedure estimated the lifetime was about 18 months (Figure 5(b) inserted). The stable photogenerated radicals for **QDU-12A** were further demonstrated by the decay curve of ESR measurements under ambient conditions (Figure S7).

The TPT ligand could also generate radicals by itself [45], however, the stability of TPT$^{\cdot}$ radicals much improved after coordination in **QDU-12A**. For **QDU-12A**, the ultra-long lifetime of photogenerated radicals was mainly originated from the two aspects. Firstly, the generated radicals were delocalized in the π-conjugated TPT ligands, diluting spin densities and leading to diminishing reactivities of photogenerated radicals. The main reason was the stacking interactions, that is to say, strong interchain π-π interactions were formed between large π-conjugated TPT ligands. The offset π-π interactions with inter-centroid distances were between 3.630(3) and 3.726(2) Å (Figure 6) for **QDU-12**. The dihedral angles between two pyridyl rings of the TPT groups were close to 0°, stabilizing the charge delocalization degree and the generated radicals. Such strong interchain π-π interactions could greatly weaken the quenching of generated radicals by oxygen at ambient condition. Moreover, the distances of interchain π-π interactions slightly decreased to 3.621(3) and 3.718(2) Å after light irradiation, providing a pronounced shielding effect towards the ultra-long stabilized radicals. In our previous work of **QDU-1** [22], even though the same π-conjugated TPT ligands were introduced in the architecture, no effective π-π interactions formed between the TPT components, then the photogenerated radicals were finally preserved for only several days in the dark at room temperature.

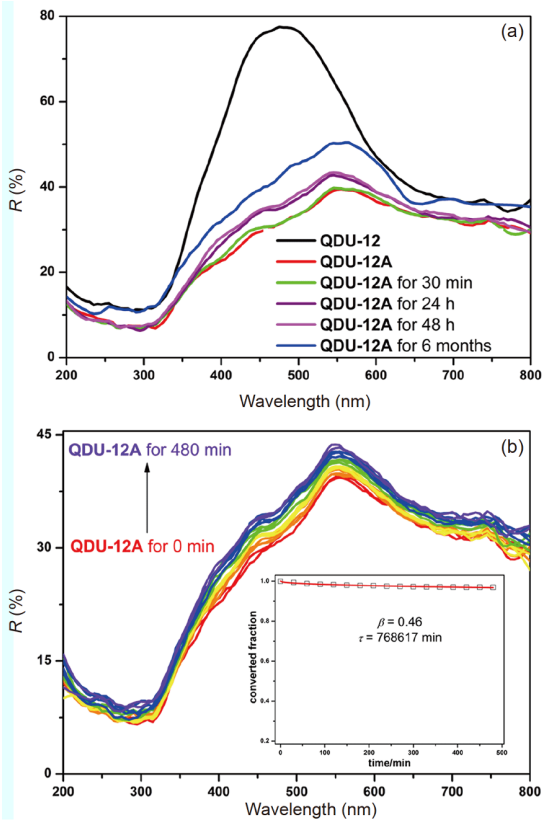

Figure 5 (a) UV-Vis diffuse-reflectance spectra for **QDU-12A** in dark at different time; (b) the decayed UV-Vis diffuse-reflectance spectra for **QDU-12A** at an interval of 30 min. The inserted curve represents the relaxation kinetics of reflective intensity at 560 nm (converted into absorbance) in normalized values (t=0 min, converted fraction=1) for **QDU-12A** in the dark at room temperature, and the red solid line presented the stretched-exponential fitted curve (color online).

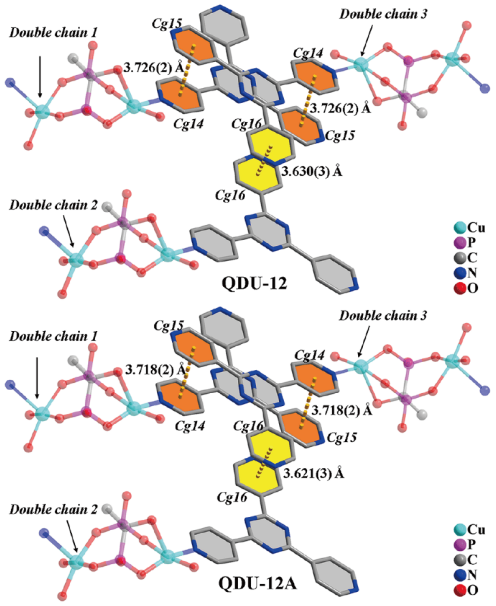

Figure 6 Interchain π-π interactions between terminal TPT ligands among the adjacent double chains for **QDU-12** and **QDU-12A** (color online).

The magnetic properties of **QDU-12** were confirmed by direct current magnetic susceptibility measurements between 2 and 300 K. As shown in Figure 7, the observed χT value at 300 K was 1.49 cm^3 K mol^{-1}, higher than the spin-only value for three isolated Cu^{2+} ions (S=1/2, g=2.0) [46]. Upon cooling, the curve sharply decreased to a minimum value of 0.62 cm^3 K mol^{-1} at 28 K, and then continuously increased to 1.79 cm^3 K mol^{-1} at 2 K, characteristic of ferrimagnetism between the Cu^{2+} centers [47]. The magnetization values in the *M-H* curve at 2 K exhibited a linear increase at low fields and then slowly reached the antiferromagnetic saturated value of 1.15 Nβ at 50 kOe (Figure S8).

Due to the generation of radicals after light irradiation, magnetic susceptibility measurements were also performed for **QDU-12A** to explore the magnetic couplings between radicals and Cu^{2+} ions. As shown in Figure 7, the χT value was 0.97 cm^3 K mol^{-1} at 300 K, drastically dropped with a colossal decrease proportion of 34.9 %, which was higher than the largest RT photodemagnetization of c.a. 33.5% in a reported 3d−4f hexacyanoferrate [48]. The magnetization anomaly should be mainly originated from the antiferromagnetic coupling between Cu^{2+} ions and photogenerated $TPT^{\cdot}$ radicals. Upon cooling, the χT values slowly decreased to a minimum of 0.49 cm^3 K mol^{-1} around 30 K and then sharply increased to 1.53 cm^3 K mol^{-1} at 2 K, similar with the tendency before irradiation. The isothermal magnetization after irradiation showed the same trend but smaller values with 0.99 Nβ at 50 kOe (Figure S8), indicating the antiferromagnetic coupling between photogenerated radicals and paramagnetic Cu^{2+} ions.

3 Conclusions

In summary, the ultra-stable radicals were realized *via* light irradiation in a sterically encumbered and π-conjugated TPT component constructed photochromic complex. The generated radicals with light-induced coloration were demonstrated by structural analyses, UV-Vis, ESR, XPS, magnetic measurements and molecular orbital calculations. The photomagnetic behavior was also performed with the largest room temperature photodemagnetization in the current radical-based photochromic materials. The radicals are protected against quenching by the strong interchain π-π interactions between the large π-conjugated TPT ligands, with the life-time of maintaining for as long as 18 months at ambient conditions, being the highest stable radicals in the reported photochromic materials. Furthermore, an anomalous demagnetization appeared after light irradiation, showing the largest demagnetization ratio in the RT photochromic materials. This work for the first time synthesized a photochromic copper(II)-diphosphonate complex with ultra-long-lived stable radicals under the participation with sterically encumbered and π-conjugated TPT component, realizing the largest RT photodemagnetization phenomenon *via* the antiferromagnetic couplings between Cu^{2+} ions and stable radicals. This work provides a platform for constructing a system to extraordinarily stabilize the generated radicals, which can arouse the future development of the optically manipulated photoelectromagnetic devices.

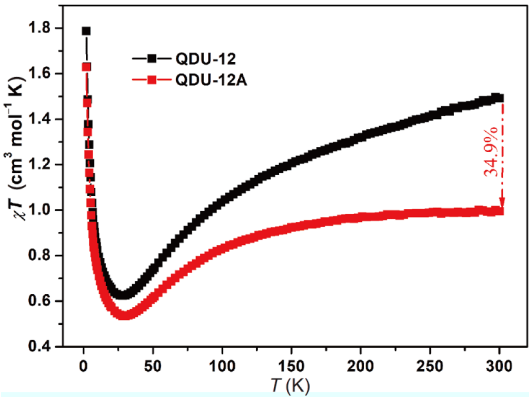

Figure 7 Temperature-dependent susceptibilities of **QDU-12** and **QDU-12A** under a dc magnetic field of 1000 Oe (color online).

Acknowledgements This work was supported by the National Natural Science Foundation of China (21901133, 22071125, 22071126, 21571111) and the Key Research and Development Project of Shandong Province (2019GGX102006). We thank for Dr Jian-Hua Qin (Luoyang Normal University, China) for the SCXRD data refinements.

Conflict of interest The authors declare no conflict of interest.

Supporting information The supporting information is available online at http://chem.scichina.com and http://link.springer.com/journal/11426. The supporting materials are published as submitted, without typesetting or editing. The responsibility for scientific accuracy and content remains entirely with the authors.

1 Ratera I, Veciana J. *Chem Soc Rev*, 2012, 41: 303–349
2 Zeng Z, Shi X, Chi C, López Navarrete JT, Casado J, Wu J. *Chem Soc Rev*, 2015, 44: 6578–6596
3 Zhou J, Zhu W, Zeng M, Yang Q, Li P, Lan L, Peng J, Li Y, Huang F, Cao Y. *Sci China Chem*, 2019, 62: 1656–1665
4 Ai X, Evans EW, Dong S, Gillett AJ, Guo H, Chen Y, Hele TJH, Friend RH, Li F. *Nature*, 2018, 563: 536–540
5 Chen X, Zhao W, Baryshnikov G, Steigerwald ML, Gu J, Zhou Y, Ågren H, Zou Q, Chen W, Zhu L. *Nat Commun*, 2020, 11: 945
6 Wang W, Wang L, Chen S, Yang W, Zhang Z, Wang X. *Sci China Chem*, 2018, 61: 300–305
7 Cui Z, Abdurahman A, Ai X, Li F. *CCS Chem*, 2020, 2: 1129–1145
8 Hu X, Chen H, Zhao L, Miao M, Zheng Y. *Chem Mater*, 2019, 31: 10256–10262
9 Miura T, Maeda K, Oka Y, Ikoma T. *J Phys Chem B*, 2018, 122: 12173–12183
10 Tang S, Zhang L, Ruan H, Zhao Y, Wang X. *J Am Chem Soc*, 2020, 142: 7340–7344
11 Ji L, Shi J, Wei J, Yu T, Huang W. *Adv Mater*, 2020, 32: 1908015
12 Meng X, Shi W, Cheng P. *Coord Chem Rev*, 2019, 378: 134–150
13 Wang Y, Hickox HP, Xie Y, Wei P, Blair SA, Johnson MK, Schaefer Iii HF, Robinson GH. *J Am Chem Soc*, 2017, 139: 6859–6862
14 Cobo S, Ostrovskii D, Bonhommeau S, Vendier L, Molnar G, Salmon

L, Tanaka K, Bousseksou A. *J Am Chem Soc*, 2008, 130: 9019–9024
15 Meng YS, Liu T. *Acc Chem Res*, 2019, 52: 1369–1379
16 Zak JK, Miyasaka M, Rajca S, Lapkowski M, Rajca A. *J Am Chem Soc*, 2010, 132: 3246–3247
17 Kato K, Osuka A. *Angew Chem Int Ed*, 2019, 58: 8978–8986
18 Wu J, Tao C, Li Y, Li J, Yu J. *Chem Sci*, 2015, 6: 2922–2927
19 Gao CY, Yang Y, Ai J, Tian HR, Li LJ, Yang W, Dang S, Sun ZM. *Chem Eur J*, 2016, 22: 11652–11659
20 Shen JJ, Li XX, Yu TL, Wang F, Hao PF, Fu YL. *Inorg Chem*, 2016, 55: 8271–8273
21 Li L, Wang JR, Hua Y, Guo Y, Fu C, Sun YN, Zhang H. *J Mater Chem C*, 2019, 7: 38–42
22 Ma YJ, Hu JX, Han SD, Pan J, Li JH, Wang GM. *J Am Chem Soc*, 2020, 142: 2682–2689
23 Li SL, Han M, Zhang Y, Li GP, Li M, He G, Zhang XM. *J Am Chem Soc*, 2019, 141: 12663–12672
24 Yu XQ, Sun C, Liu BW, Wang MS, Guo GC. *Nat Commun*, 2020, 11: 1179
25 Mallick A, Garai B, Addicoat MA, Petkov PS, Heine T, Banerjee R. *Chem Sci*, 2015, 6: 1420–1425
26 Bonanno NM, Lough AJ, Lemaire MT. *Inorg Chem*, 2018, 57: 4837–4840
27 Cheng L, Zhao JW, Yang GY. *Dalton Trans*, 2014, 43: 7324–7330
28 Jiao CQ, Zhao Z, Ma C, Sun ZG, Dong DP, Zhu YY, Li J. *Cryst Growth Des*, 2016, 16: 5624–5635
29 Dessapt R, Collet M, Coue V, Bujoli-Doeuff M, Jobic S, Lee C, Whangbo MH. *Inorg Chem*, 2009, 48: 574–580
30 Ma P, Hu F, Wan R, Huo Y, Zhang D, Niu J, Wang J. *J Mater Chem C*, 2016, 4: 5424–5433
31 Sun JK, Yang XD, Yang GY, Zhang J. *Coord Chem Rev*, 2019, 378: 533–560
32 Zhang CJ, Chen ZW, Lin RG, Zhang MJ, Li PX, Wang MS, Guo GC. *Inorg Chem*, 2014, 53: 847–851
33 Kavarnos GJ, Turro NJ. *Chem Rev*, 1986, 86: 401–449
34 Matsuda K, Takayama K, Irie M. *Inorg Chem*, 2004, 43: 482–489
35 Liu J. *Dyes Pigments*, 2019, 160: 476–482
36 Li SL, Li M, Zhang Y, Xu HM, Zhang XM. *Inorg Chem*, 2020, 59: 9047–9054
37 Ma YJ, Han SD, Pan J, Mu Y, Li JH, Wang GM. *J Mater Chem C*, 2018, 6: 9341–9344
38 Gong T, Li P, Sui Q, Zhou LJ, Yang NN, Gao EQ. *Inorg Chem*, 2018, 57: 6791–6794
39 Ma YJ, Hu JX, Han SD, Pan J, Li JH, Wang GM. *Chem Commun*, 2019, 55: 5631–5634
40 Xia B, Zhou Y, Wang QL, Xu XF, Tong YZ, Bu XH, Li JR. *Dalton Trans*, 2018, 47: 15888–15896
41 Gong T, Yang X, Sui Q, Qi Y, Xi FG, Gao EQ. *Inorg Chem*, 2016, 55: 96–103
42 Wang J, Li SL, Zhang XM. *ACS Appl Mater Interfaces*, 2016, 8: 24862–24869
43 Jin XH, Wang J, Sun JK, Zhang HX, Zhang J. *Angew Chem Int Ed*, 2011, 50: 1149–1153
44 Jiang W, Jiao C, Meng Y, Zhao L, Liu Q, Liu T. *Chem Sci*, 2018, 9: 617–622
45 Zhang N, Han Y, Du M, Sa R, Wang M, Guo G. *Chem Eur J*, 2019, 25: 13972–13976
46 Cai LZ, Jiang XM, Zhang ZJ, Guo PY, Jin AP, Wang MS, Guo GC. *Inorg Chem*, 2017, 56: 1036–1040
47 Yin P, Zheng LM, Gao S, Xin XQ. *Chem Commun*, 2001, 37: 2346–2347
48 Cai LZ, Chen QS, Zhang CJ, Li PX, Wang MS, Guo GC. *J Am Chem Soc*, 2015, 137: 10882–10885